Chinese Physics Letters

LETTER

Magnetization-Induced Higher-Order Topological Effects in Quantum Spin Hall Insulators

Cite as: Xiang-Long Yu *et al*. 2026 *Chin. Phys. Lett.* **43** 070710

DOI CSTR

Recommended Articles

Observation of Topological Hall Effect and Nernst Effect in the Canted Antiferromagnetic Phase of $MnBi_2Te_4$

Haiyang Yang *et al*.
Chin. Phys. Lett. **42**, 080706 (2025)

From Topological Nodal-Line Semimetals to Quantum Spin Hall Insulators in Tetragonal SnX Monolayers (X=F, Cl, Br, I)

Ye Zhu, Bao Zhao, Yang Xue, Wei Xu, Wenting Xu, and Zhongqin Yang
Chin. Phys. Lett. **41**, (2024)

Prediction of the Dual Quantum Spin Hall Insulator in the $NbIrTe_4$ Monolayer

Xiangyang Liu, Junwen Lai, Jie Zhan, Tianye Yu, Wujun Shi, Peitao Liu, Xing-Qiu Chen, and Yan Sun
Chin. Phys. Lett. **42**, 037302 (2025)

Hybridization Gap and Edge States in Strained-Layer InAs/$In_{0.5}Ga_{0.5}Sb$ Quantum Spin Hall Insulator

Wenfeng Zhang, Peizhe Jia, Wen-kai Lou, Xinghao Wang, Shaokui Su, Kai Chang, and Rui-Rui Du
Chin. Phys. Lett. **43**, 010704 (2026)

Observation of Giant Topological Hall Effect in Room-Temperature Ferromagnet $Cr_{0.82}Te$

Wei-Ting Miao, Wei-Li Zhen, Zhen Lu, Heng-Ning Wang, Jie Wang, Qun Niu, and Ming-Liang Tian
Chin. Phys. Lett. **41**, (2024)

Higher-Order Topological States in Chiral Split Magnons of Honeycomb Altermagnets

Xuan Guo, Meng-Han Zhang, and Dao-Xin Yao
Chin. Phys. Lett. **42**, 120703 (2025)

A series journal of Chinese Physical Society distributed by IOP Publishing

Chinese Physics Letters

Chin. Phys. Lett. 43 070710 (2026)

LETTER

DOI: 10.1088/0256-307X/43/7/070710
CSTR: 32039.14.0256-307X.43.7.070710

Magnetization-Induced Higher-Order Topological Effects in Quantum Spin Hall Insulators

Xiang-Long Yu(虞祥龙)[1,†], Jie Wang(王洁)[2,†], Pei-Hao Fu(傅培浩)[1,*], Da-Yong Liu(刘大勇)[2,*], and Dao-Xin Yao(姚道新)[3,*]

[1]School of Science, Sun Yat-sen University, Shenzhen 518107, China
[2]School of Physical Science and Technology, Nantong University, Nantong 226019, China
[3]Guangdong Provincial Key Laboratory of Magnetoelectric Physics and Devices, State Key Laboratory of Optoelectronic Materials and Technologies, School of Physics, Sun Yat-sen University, Guangzhou 510275, China

[†]These authors contributed equally to this work.
[*]Corresponding authors. Email: phy.phfu@gmail.com; dyliu@ntu.edu.cn; yaodaox@mail.sysu.edu.cn

Higher-order topological phases offer a promising platform for low-dissipation electronic and spintronic devices, motivating the search for experimentally accessible control schemes. Here we investigate higher-order topological states in a rhombic geometry of two-dimensional group-IV*A* materials subjected to external magnetic fields, described by a modified Kane–Mele model with next-nearest-neighbor Rashba spin–orbit coupling. We identify two distinct types of corner modes governed by different physical mechanisms: under out-of-plane magnetization, corner states emerge at the acute angles due to boundary hybridization induced by spin–orbit coupling, whereas under in-plane magnetization, corner modes appear at the obtuse angles as topologically protected Jackiw–Rebbi solitons arising at the domain wall between boundaries with different topological invariants. Using first-principles-based parameters for realistic materials including silicene, germanene, and stanene, we show that the obtuse-angle corner states are robust and enhanced in systems with stronger spin–orbit coupling. Our results establish a feasible route for magnetically creating and controlling higher-order topological states, enabling reconfigurable corner-mode-based topological devices.

Introduction

Topological materials are characterized by topological boundary modes that enable dissipationless or low-dissipation electronic transport [1−8]. By definition, a d-dimensional system hosting $(d-n)$-dimensional gapless boundary states, with $1<n\leq d$ $(n\in\mathbb{Z})$, is classified as an n^{th}-order topological system [9−11]. Following extensive progress on so-called first-order topological insulators [12,13] and semimetals [14,15], increasing attention has been devoted to higher-order topological phases with $1<n\leq d$ [16−20]. Higher-order topological phases have been theoretically predicted and experimentally realized in both insulating and superconducting systems [21−24]. Representative realizations include corner and hinge modes in higher-order topological insulators [9,10,17−19,24−29], as well as Majorana corner modes in second-order topological superconductors [30−32]. Among these, topological corner modes in two-dimensional (2D) second-order topological insulators are of particular interest, having been observed in diverse lattice geometries, including tetragonal, honeycomb, and kagome structures [33−42], and offering promising opportunities for topological electronics, spintronics, and quantum computation. Engineering higher-order topological phases is therefore a central objective in topological matter research. External magnetic fields and induced magnetization have emerged as effective means to generate and manipulate nontrivial topology [1,14,43]. Recent studies have demonstrated magnetization-induced higher-order topological phases [18,44−46], in $Bi_{2-x}Sm_xSe_3$ [47,48] and bismuthene [49].

Despite these advances, the experimental realization of higher-order topological phases remains challenging due to material constraints and the difficulty of probing boundary signatures [19,30,46,47,49−53]. More critically, a clear theoretical understanding of the physical mechanisms governing magnetization-controlled corner states is still lacking, hindering systematic material design and device implementation. In this work, we investigate higher-order topological states in a rhombic geometry of 2D group-IV*A* materials under external magnetic fields, described by a modified Kane–Mele Hamiltonian with next-nearest-neighbor (NNN) Rashba spin–orbit coupling (SOC) [3,54]. We identify two distinct types of corner modes arising from different mechanisms: under out-of-plane magnetization, corner states emerge at acute angles due to boundary hybridization induced by SOC, whereas under in-plane magnetization, corner states appear at obtuse angles as topologically protected Jackiw–Rebbi solitons [55] originating from discontinuities in boundary topological invariants. Using first-principles-based parameters for realistic group-IV*A* materials [54,56], we further demonstrate that the obtuse-angle corner states are robust and enhanced in systems with stronger SOC. These results establish an experimentally feasible route to magnetically realizing and controlling higher-order topological states, enabling reconfigurable corner-mode-based topological devices.

Model Hamiltonian

We consider a general four-band effective model describing 2D group-IV*A* materials with a buckled honeycomb lattice [3,54,56−66], as illustrated in Fig. 1. In the presence of a Zeeman field, the Hamiltonian reads [56,67−70]

$$H = H_{\text{KM}} + H_{\text{Z}}, \tag{1}$$

with

$$\begin{aligned} H_{\text{KM}} = &-t\sum_{\langle i,j\rangle} c^{\dagger}_{i\sigma}c_{j\sigma} + \mathrm{i}\lambda_{\text{SO}}\sum_{\langle\langle i,j\rangle\rangle,\alpha\beta}\nu_{ij}c^{\dagger}_{i\alpha}\sigma^{z}_{\alpha\beta}c_{j\beta} \\ &+\mathrm{i}\lambda_{\text{R}}\sum_{\langle\langle i,j\rangle\rangle,\alpha\beta}u_{ij}c^{\dagger}_{i\alpha}(\boldsymbol{\sigma}\times\boldsymbol{d}_{ij})^{z}_{\alpha\beta}c_{j\beta} + \text{H.c.}, \end{aligned} \tag{2}$$

and

$$H_{\text{Z}} = \lambda_{\text{B}}\sum_{i,\alpha\beta} c^{\dagger}_{i\alpha}(\boldsymbol{B}\cdot\boldsymbol{\sigma})_{\alpha\beta}c_{i\beta}. \tag{3}$$

Received 14 April 2026; accepted 1 July 2026; published 22 July 2026

© 2026 Chinese Physical Society and IOP Publishing Ltd. All rights, including for text and data mining, AI training, and similar technologies, are reserved.

Check for updates

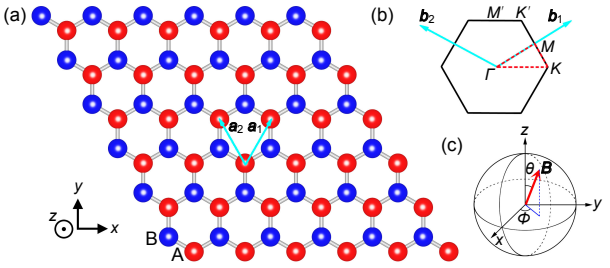

Fig. 1. (a) Buckled honeycomb lattice with A (red) and B (blue) sublattices; $\boldsymbol{a}_1$ and $\boldsymbol{a}_2$ denote primitive lattice vectors. (b) First Brillouin zone showing high-symmetry points and paths, with reciprocal vectors $\boldsymbol{b}_1$ and $\boldsymbol{b}_2$. (c) Magnetization direction $\boldsymbol{B}$ defined by polar angle θ and azimuthal angle ϕ.

Equation (2) is the Kane–Mele Hamiltonian for a quantum spin Hall insulator (QSHI) [3,54], including nearest-neighbor hopping t, intrinsic SOC λ_{SO}, and Rashba SOC λ_{R}. Here, ν_{ij} denotes the hopping chirality between sites j and i, while $u_{ij} = \pm 1$ labels the A and B sublattices. Equation (3) describes the Zeeman coupling to an external or exchange field $\boldsymbol{B} = (\sin\theta\cos\phi, \sin\theta\sin\phi, \cos\theta)$, with θ and ϕ the polar and azimuthal angles, respectively, see Fig. 1(c). $\boldsymbol{\sigma} = (\sigma_x, \sigma_y, \sigma_z)$ are Pauli matrices, and t is taken as the energy unit.

Originally introduced as a minimal model for QSHIs, equation (2) has been shown to quantitatively describe a wide range of 2D group-IVA materials [3,54,56–66]. Equation (1) therefore provides a unified framework for studying magnetically controlled topological corner modes. In the following, we analyze corner states induced by out-of-plane and in-plane magnetizations and subsequently extend the discussion to general non-axial configurations.

Magneto-Engineering Topological Corner Modes

We first consider the QSHI phase described by Eq. (1) under an out-of-plane magnetization, with $\lambda_{\mathrm{SO}} = \lambda_{\mathrm{R}} = 0.3t$, $\lambda_{\mathrm{B}} = 0.3t$, and $\theta = 0$. As shown in Fig. 2(a), the bulk and nanoribbon spectra exhibit gaps of about 1.40 eV and 0.22 eV, respectively, with the latter corresponding to an edge-state gap embedded within the bulk gap. The nontrivial topology is confirmed by the Wannier function center (WFC) evolution [71,72], which shows an odd number of crossings, as well as by the presence of four edge-derived bands inside the bulk gap, indicating a time-reversal-symmetry-broken QSH phase [69]. Finite-size calculations [Fig. 2(b)] reveal two in-gap states within the nanoribbon gap. Because magnetic perturbations break spin-rotation symmetry, these states are generally gapped [49,73,74]. Their weight distributions are strongly localized at the acute-angle intersections of zigzag edges, identifying them as zero-dimensional (0D) corner states, in contrast to other in-gap states that remain extended along the edges.

Applying an in-plane magnetization along the x direction ($\phi = 0$) with the same parameters yields qualitatively similar bulk topology [Fig. 2(c)], but only two edge bands appear within the bulk gap and the nanoribbon gap increases to $\sim$0.33 eV at $k_x = \pi$. This reduction of edge-band multiplicity arises because the in-plane magnetization aligns with the nanoribbon direction, preserving edge-state degeneracy. The corresponding finite-size spectrum [Fig. 2(d)] again hosts two in-gap states, whose weights are now localized at the obtuse-angle corners, representing a distinct pair of 0D corner modes. Results for $\phi \neq 0$ show the same qualitative behavior and are provided in the Supplementary Material (SM) [71].

To elucidate the general evolution of corner states under non-axial magnetization, figure 2(e) maps the dominant weight positions of the two in-gap states as functions of the polar angle θ and azimuthal angle ϕ. For small θ, the corner-state weight is concentrated at the acute angles; with increasing θ, the states delocalize onto the boundaries and subsequently reappear at the obtuse angles for sufficiently large θ. The intermediate region corresponds to a boundary-dominated regime connecting the two corner phases. The azimuthal angle ϕ mainly controls the direction along which the weight is redistributed between opposite edges, without generating additional corner states. Animations, full phase diagrams, and energy-gap evolutions as functions of λ_{B}, θ, and ϕ are presented in the SM [71]. Overall, while the magnetization strength λ_{B} sets the bulk and nanoribbon gap scales, the magnetization orientation governs the position and evolution of the corner modes, enabling controlled and reversible manipulation of higher-order boundary states.

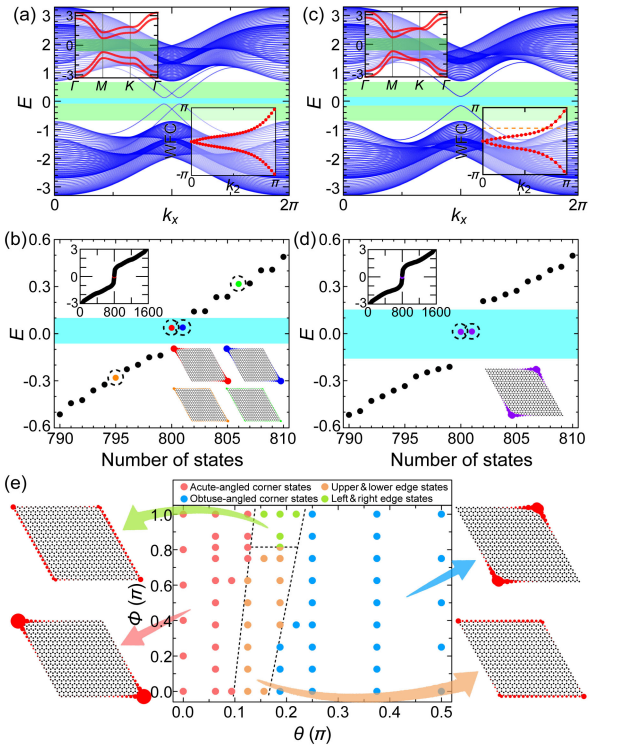

Fig. 2. (a) Band structure of a nanoribbon (width: 20 zigzag chains) under an out-of-plane magnetization, with $\lambda_{\mathrm{SO}} = 0.3$, $\lambda_{\mathrm{R}} = 0.3$, $\lambda_{\mathrm{B}} = 0.3$, and $\theta = 0$. The bulk and nanoribbon gaps are indicated by green and blue shading, respectively. Insets: The corresponding bulk band structure and the evolution curves of the Wannier function center. The orange dashed line serves as a reference line. (b) Partial energy levels of a finite-size system (20×20 unit cells) under the same parameters. Insets: Complete energy spectrum and spatial probability distributions of the four states marked by dashed circles and corresponding colors. The size of the filled circle represents the weight of the particle state, normalized here and in the subsequent figures. (c) and (d) Analogous to (a) and (b), but for an in-plane magnetization with $\theta = \pi/2$, and $\phi = 0$. (e) Schematic phase diagram illustrating the dominant weight positions of the two intermediate states (Nos. 800 and 801) in the finite system. Each solid dot represents a calculated data point.

Physical Origin of Corner States

To elucidate the origin of the corner states, we construct an effective one-dimensional (1D) boundary model describing magnetized edge states [71]. In momentum space, the Hamiltonian reads $H_{1\mathrm{D}} = d \cdot \boldsymbol{\sigma}$ with $d_x = \lambda_{\mathrm{B}} \sin\theta\cos\phi$, $d_y = -2\lambda_{\mathrm{R}}^{\mathrm{eff}} \sin k + \lambda_{\mathrm{B}} \sin\theta\sin\phi$, and $d_z = 2\lambda_{\mathrm{SO}}^{\mathrm{eff}} \sin k + \lambda_{\mathrm{B}} \cos\theta$, where $\lambda_{\mathrm{SO}}^{\mathrm{eff}}$ and $\lambda_{\mathrm{R}}^{\mathrm{eff}}$ are effective intrinsic and Rashba SOCs. Near $k = 0$, this model reproduces the edge dispersions of the full Kane–Mele Hamiltonian, including the magnetization-induced gap opening [Figs. 3(a) and 3(c)]. The topology of the boundary model is characterized by the Zak phase [75]. Since d_x is momentum independent, the invariant can be evaluated by neglecting this term [71], yielding

$$Z = \mathrm{sgn}[\lambda_{\mathrm{B}}(\lambda_{\mathrm{SO}}^{\mathrm{eff}} \sin\theta\sin\phi + \lambda_{\mathrm{R}}^{\mathrm{eff}} \cos\theta)]\pi. \tag{4}$$

Equation (4) shows that the boundary topology depends jointly on SOC and magnetization direction. Because $\lambda_{\mathrm{SO}}^{\mathrm{eff}}$ and $\lambda_{\mathrm{R}}^{\mathrm{eff}}$ have opposite signs on A- and B-terminated edges, the corresponding 1D

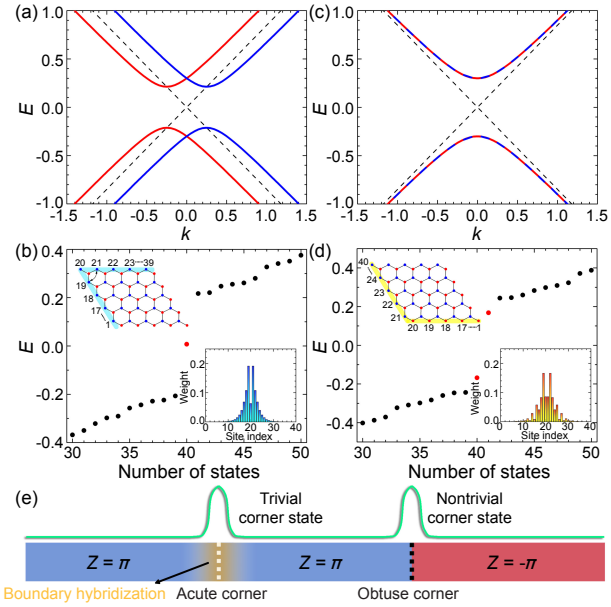

Fig. 3. Band structure of edge states with (a) out-of-plane and (c) in-plane magnetization. The red and blue solid lines respectively represent the A and B sublattices, and the dashed thin black lines denote the degenerated dispersion without magnetization. (b) and (d) Energy and spatial distribution of the topological corner modes at acute and obtuse intersections of zigzag edges, respectively. Parameters: same as Fig. 2. (e) Schematic illustration of the physical mechanisms underlying corner-state formation at acute and obtuse angles. The white and black dashed lines denote the acute and obtuse corners, respectively. Blue and red backgrounds correspond to boundaries with opposite Zak phases. The orange annotation at the acute corner indicates boundary hybridization. The green line schematically illustrates the two types of corner states.

boundaries generally carry opposite Zak phases. In particular, $Z = \mathrm{sgn}(\lambda_{\mathrm{R}}^{\mathrm{eff}})\pi$ for out-of-plane magnetization ($\theta = 0$) and $Z = \mathrm{sgn}(\lambda_{\mathrm{SO}}^{\mathrm{eff}})\pi$ for in-plane magnetization ($\theta = \pi/2$, $0 < \phi < \pi$). This framework clarifies the two types of corner states observed in Fig. 2. For out-of-plane magnetization, corner states appear at acute intersections of zigzag edges [Fig. 3(b)]. These states originate from hybridization H_{acu} between two boundaries with identical sublattice termination and identical topological invariants; removing the hybridization eliminates the in-gap state [71], confirming its topologically trivial nature. By contrast, for in-plane magnetization, corner states emerge at obtuse angles [Fig. 3(c)], where an A-terminated boundary meets a B-terminated one [Fig. 3(d)]. According to Eq. (4), the two boundaries carry opposite Zak phases ($Z = \pm\pi$), and their interface hosts Jackiw–Rebbi-type topological bound states [55].

To provide a more intuitive illustration of the physical mechanism underlying the formation of corner states, we present a schematic diagram in Fig. 3(e). It can be seen that the two edges meeting at the acute corner share the same Zak phase, and the acute-angle corner states arise from boundary hybridization, making them topologically trivial. In contrast, the two edges meeting at the obtuse corner possess different Zak phases, which leads to the formation of topologically protected Jackiw–Rebbi-type bound states at the obtuse corner. Furthermore, analysis of the bulk Hamiltonian along symmetry-preserving lines shows that the in-plane-magnetized system decomposes into two 1D subsystems with winding numbers $\nu^{\pm} = \pm 1$ in the absence of NNN Rashba SOC, confirming their topological distinction [71]. Although NNN Rashba SOC breaks mirror and chiral symmetries, it does not close the bulk or nanoribbon gaps, and the obtuse-angle corner modes persist, thereby constituting an extrinsic higher-order topological phase [71,76] where the topology is induced by the boundary configuration and protected by the bulk and edge gaps, rather than by crystalline symmetries.

Discussion and Conclusion

Our results clarify the magnetization-controlled corner physics of group-IV*A* materials and distinguish it from earlier studies. Unlike bismuthene, where in-plane magnetization induces multiple corner states simultaneously [49], group-IV*A* systems host acute- and obtuse-angle corner modes separately under out-of-plane and in-plane magnetizations due to distinct physical mechanisms. Specifically, obtuse-angle corner states arise from topological mismatch between inequivalent boundaries and constitute genuine interface modes [1,75], whereas acute-angle corner states originate from boundary hybridization and are topologically trivial [76–78]. Directional control of magnetization in a rhombic geometry therefore enables selective realization and positioning of different corner modes, a feature robust against variations in boundary termination.

We further demonstrate that these mechanisms persist in realistic group-IV*A* materials using first-principles-based parameters. In particular, under in-plane magnetization corner-like states initially form along the edges and progressively localize at the obtuse angles as the magnetization increases, with the degree of spatial separation controlled primarily by the intrinsic SOC; full material-specific results are provided in the SM [71]. Overall, using a magnetized Kane–Mele model and an effective 1D boundary theory, we establish a unified framework for understanding and manipulating higher-order corner states, highlighting magnetic-field orientation as a practical and reversible control knob for reconfigurable higher-order topological systems and devices.

Acknowledgements

This work was supported by the National Natural Science Foundation of China (Grant No. 11974354), the Shenzhen Science and Technology Program (Grant No. JCYJ20250604174400001), and the Basic Start-up Fund for Introduced Talents at Sun Yat-sen University.

References

[1] Hasan M Z and Kane C L 2010 *Rev. Mod. Phys.* **82** 3045
[2] Yan Z B 2019 *Acta Phys. Sin.* **68** 226101
[3] Kane C L and Mele E J 2005 *Phys. Rev. Lett.* **95** 146802
[4] Bernevig B A, Hughes T L, and Zhang S C 2006 *Science* **314** 1757
[5] Bercioux D, Cayssol J, Vergniory M G, and Reyes Calvo M eds. 2018 *Topological Matter: Lectures from the Topological Matter School 2017* (Springer Cham)
[6] Zhang Z Z, Chang K, and Peeters F M 2008 *Phys. Rev. B* **77** 235411
[7] Huang A, Ke S, Guan J H, Li J, and Lou W K 2024 *Phys. Rev. B* **109** 045408
[8] Huang A, Ke S, Guan J H, Li J, and Lou W K 2024 *Chin. Phys. Lett.* **41** 097302
[9] Benalcazar W A, Bernevig B A, and Hughes T L 2017 *Phys. Rev. B* **96** 245115
[10] Benalcazar W A, Bernevig B A, and Hughes T L 2017 *Science* **357** 61
[11] Song Z, Fang Z, and Fang C 2017 *Phys. Rev. Lett.* **119** 246402
[12] Onoda M and Nagaosa N 2003 *Phys. Rev. Lett.* **90** 206601
[13] Kane C L and Mele E J 2005 *Phys. Rev. Lett.* **95** 226801
[14] Armitage N P, Mele E J, and Vishwanath A 2018 *Rev. Mod. Phys.* **90** 015001
[15] Wan X, Turner A M, Vishwanath A, and Savrasov S Y 2011 *Phys. Rev. B* **83** 205101
[16] Schindler F, Cook A M, Vergniory M G, Wang Z J, Parkin S S P, Bernevig B A, and Neupert T 2018 *Sci. Adv.* **4** eaat0346
[17] Langbehn J, Peng Y, Trifunovic L, von Oppen F, and Brouwer P W 2017 *Phys. Rev. Lett.* **119** 246401
[18] Ezawa M 2018 *Phys. Rev. B* **97** 155305
[19] Wang Z J, Wieder B J, Li J, Yan B H, and Bernevig B A 2019 *Phys. Rev. Lett.* **123** 186401
[20] Hua C and Xu D H 2025 *Chin. Phys. B* **34** 037301
[21] Wu Z, Yan Z, and Huang W 2019 *Phys. Rev. B* **99** 020508
[22] Yan Z 2019 *Phys. Rev. Lett.* **123** 177001
[23] Kheirkhah M, Yan Z, Nagai Y, and Marsiglio F 2020 *Phys. Rev. Lett.* **125** 017001

[24] Zhu D, Kheirkhah M, and Yan Z 2023 *Phys. Rev. B* **107** 085407
[25] Zhang F, Kane C L, and Mele E J 2013 *Phys. Rev. Lett.* **110** 046404
[26] Sitte M, Rosch A, Altman E, and Fritz L 2012 *Phys. Rev. Lett.* **108** 126807
[27] Lin Z K, Wu S Q, Wang H X, and Jiang J H 2020 *Chin. Phys. Lett.* **37** 074302
[28] Zhang Y, Hu Y, Li Y, and Shang C 2026 *Chin. Phys. Lett.* **43** 010403
[29] Lü S and Hu J 2025 *Chin. Phys. B* **34** 117303
[30] Yan Z 2019 *Phys. Rev. B* **100** 205406
[31] Yan Z, Song F, and Wang Z 2018 *Phys. Rev. Lett.* **121** 096803
[32] Zhu X 2018 *Phys. Rev. B* **97** 205134
[33] Peterson C W, Benalcazar W A, Hughes T L, and Bahl G 2018 *Nature* **555** 346
[34] Serra-Garcia M, Peri V, Susstrunk R, Bilal O R, Larsen T, Villanueva L G, and Huber S D 2018 *Nature* **555** 342
[35] Imhof S, Berger C, Bayer F, Brehm J, Molenkamp L W, Kiessling T, Schindler F, Lee C H, Greiter M, Neupert T, and Thomale R 2018 *Nat. Phys.* **14** 925
[36] Xue H R, Yang Y H, Gao F, Chong Y D, and Zhang B L 2019 *Nat. Mater.* **18** 108
[37] Ni X, Weiner M, Alu A, and Khanikaev A B 2019 *Nat. Mater.* **18** 113
[38] Zhang X J, Wang H X, Lin Z K, Tian Y, Xie B Y, Lu M H, Chen Y F, and Jiang J H 2019 *Nat. Phys.* **15** 582
[39] Xie B Y, Wang H F, Wang H X, Zhu X Y, Jiang J H, Lu M H, and Chen Y F 2018 *Phys. Rev. B* **98** 205147
[40] Xie B Y, Su G X, Wang H F, Su H, Shen X P, Zhan P, Lu M H, Wang Z L, and Chen Y F 2019 *Phys. Rev. Lett.* **122** 233903
[41] Chen X D, Deng W M, Shi F L, Zhao F L, Chen M, and Dong J W 2019 *Phys. Rev. Lett.* **122** 233902
[42] Fan H Y, Xia B Z, Tong L, Zheng S J, and Yu D J 2019 *Phys. Rev. Lett.* **122** 204301
[43] Wang D, Chen Y, Niu Z C, and Lou W K 2024 *Chin. Phys. Lett.* **41** 087101
[44] Guo X, Zhang M H, and Yao D X 2025 *Chin. Phys. Lett.* **42** 120703
[45] Khalaf E 2018 *Phys. Rev. B* **97** 205136
[46] Kheirkhah M, Yan Z, and Marsiglio F 2021 *Phys. Rev. B* **103** L140502
[47] Yue C M, Xu Y F, Song Z D, Weng H M, Lu Y M, Fang C, and Dai X 2019 *Nat. Phys.* **15** 577
[48] Shi L K and Lou W K 2014 *Chin. Phys. Lett.* **31** 067304
[49] Han B, Zeng J J, and Qiao Z H 2022 *Chin. Phys. Lett.* **39** 017302
[50] Schindler F, Wang Z J, Vergniory M G, Cook A M, Murani A, Sengupta S, Kasumov A Y, Deblock R, Jeon S, Drozdov I, Bouchiat H, Gueron S, Yazdani A, Bernevig B A, and Neupert T 2018 *Nat. Phys.* **14** 918
[51] Xu Y F, Song Z D, Wang Z J, Weng H M, and Dai X 2019 *Phys. Rev. Lett.* **122** 256402
[52] Sheng X L, Chen C, Liu H Y, Chen Z Y, Zhao Y X, Yu Z M, and Yang S Y A 2019 *Phys. Rev. Lett.* **123** 256402
[53] Lee E, Kim R, Ahn J, and Yang B J 2020 *npj Quantum Mater.* **5** 1
[54] Liu C C, Jiang H, and Yao Y G 2011 *Phys. Rev. B* **84** 195430
[55] Jackiw R and Rebbi C 1976 *Phys. Rev. D* **13** 3398
[56] Tsai W F, Huang C Y, Chang T R, Lin H, Jeng H T, and Bansil A 2013 *Nat. Commun.* **4** 1500
[57] Soodchomshom B 2014 *J. Appl. Phys.* **115** 023706
[58] Rachel S and Ezawa M 2014 *Phys. Rev. B* **89** 195303
[59] Ezawa M 2012 *Phys. Rev. Lett.* **109** 055502
[60] Ezawa M 2015 *J. Phys. Soc. Jpn.* **84** 121003
[61] Ezawa M 2012 *New J. Phys.* **14** 033003
[62] Ezawa M 2013 *Phys. Rev. B* **87** 155415
[63] Tahir M and Schwingenschlögl U 2013 *Sci. Rep.* **3** 1075
[64] Tahir M and Schwingenschlögl U 2012 *Appl. Phys. Lett.* **101** 132412
[65] Hattori A, Tanaya S, Yada K, Araidai M, Sato M, Hatsugai Y, Shiraishi K, and Tanaka Y 2017 *J. Phys. Condens. Matter* **29** 115302
[66] Ren Y, Qiao Z, and Niu Q 2016 *Rep. Prog. Phys.* **79** 066501
[67] Xiao C, Wu W, Wang H, Huang Y X, Feng X, Liu H, Guo G Y, Niu Q, and Yang S A 2023 *Phys. Rev. Lett.* **130** 166302
[68] Zhao X, Wang Z, Chen J, and Wang B 2023 *J. Phys. Condens. Matter* **35** 095401
[69] Yu X L, Fu P H, and Wu J 2022 *Phys. Rev. B* **105** 125107
[70] Wang J, Liu D Y, and Yu X L 2026 *Int. J. Mod. Phys. C* **37** 2550110
[71] See the Supplementary Material and a video at [http://dx.doi.org/10.1088/0256-307X/43/7/070710] for details on: (i) bulk/nanoribbon properties (band structures, energy levels, corner states) in the modified Kane–Mele model under various magnetizations; (ii) an effective 1D model analysis; (iii) topological corner states in realistic group-IVA materials; and (iv) structures with different boundary types.
[72] Yu R, Qi X L, Bernevig A, Fang Z, and Dai X 2011 *Phys. Rev. B* **84** 075119
[73] Wang B, Hung Y C, Zhou X, Bansil A, and Lin H 2023 *Phys. Rev. B* **108** 245103
[74] Spurrier S and Cooper N R 2020 *Phys. Rev. Res.* **2** 033071
[75] Asbóth J K, Oroszlány L, and Pályi A 2016 *A Short Course on Topological Insulators: Band Structure and Edge States in One and Two Dimensions* (Springer Cham)
[76] Trifunovic L and Brouwer P W 2019 *Phys. Rev. X* **9** 011012
[77] Yu X L and Wu J 2021 *Phys. Rev. B* **103** 205143
[78] Hu T, Zhong W, Zhang T, Wang W, and Wang Z F 2023 *Nat. Commun.* **14** 7092